Journal of Materials Chemistry

PAPER

Versatile double hydrophilic block copolymer: dual role as synthetic nanoreactor and ionic and electronic conduction layer for ruthenium oxide nanoparticle supercapacitors†

Eunyong Seo, Taemin Lee, Kyu Tae Lee, Hyun-Kon Song and Byeong-Su Kim*

The facile synthetic approach to ruthenium oxide nanoparticles using double hydrophilic block copolymers (DHBCs) and their application toward the supercapacitor are presented. Nanostructured hydrous ruthenium oxide (RuO$_2$) nanoparticles are synthesized using a double hydrophilic block copolymer of poly(ethylene oxide)-*block*-poly(acrylic acid) (PEO-*b*-PAA) as a template, forming a micelle upon addition of the ruthenium precursor, which then transformed into RuO$_2$ nanoparticles of controlled dimension with reducing agents. The synthesized hydrous RuO$_2 \cdot x$H$_2$O nanoparticles are very stable for several months without any noticeable aggregates. Furthermore, we have demonstrated their utility in application as supercapacitors. Through annealing at 400 °C, we found that the crystallinity of RuO$_2$ nanoparticles increases considerably with a simultaneous transformation of the surrounding double hydrophilic block copolymer into ionic and electronic conducting buffer layers atop RuO$_2$ nanoparticles, which contribute to the significant enhancement of the overall specific capacitance from 106 to 962 F g^{-1} at 10 mV s^{-1}. The RuO$_2$ nanoparticles annealed at 400 °C also exhibit a superior retention of capacitance over 1000 cycles at very high charge–discharge rates at 20 A g^{-1}. We envision that the double hydrophilic block copolymer will provide a facile and general tool in creating functional nanostructures with controlled dimensions that are useful for various applications.

1. Introduction

Supercapacitors are attracting considerable attention as attractive electrochemical energy storage and conversion devices with the growing demand for future portable devices and electric vehicles due to their complementary performance with respect to secondary batteries and fuel cells.[1–6] Compared with other power sources like secondary batteries, supercapacitors exhibit a number of distinctive features such as higher power density (10 kW kg^{-1}), faster charge–discharge capability (within seconds), long cycle life (>10^5), wide thermal operating range, and low maintenance cost.[7]

Depending on their charge storage mechanism and the active materials used, supercapacitors are generally classified into two major types: (1) electric double-layer capacitors (EDLCs) which store the electrical charges at the interface of a porous electrode (typically, carbon-based materials) and an electrolyte based on the non-Faradaic reaction and (2) pseudocapacitors which utilize the Faradaic reaction of redox-active materials such as conducting polymers and metal oxides. Among various electrode materials, ruthenium oxide (RuO$_2$) based supercapacitors are clearly noteworthy, displaying superior specific capacitance, and reversible charge–discharge feature with a good electrical conductivity, despite their high cost.[8–12]

It has been suggested that the electrical and electrochemical properties of RuO$_2$-based materials are highly dependent on their degree of crystallinity, hydration, and surface area. For instance, amorphous and hydrous ruthenium oxide (RuO$_2 \cdot x$H$_2$O) exhibited a superior specific capacitance of 600–900 F g^{-1} by virtue of highly reversible redox transitions based on the high proton conductivity near the interface with the electrolyte, while that of crystalline and anhydrous RuO$_2$ is only about 200 F g^{-1}.[13–16] Nevertheless, the relatively low electronic conductivity of hydrous RuO$_2 \cdot x$H$_2$O (89 S cm^{-1}) is still an obstacle to balance the electronic and proton conduction channels for achieving a high power supercapacitor electrode.

In order to address these issues, recent progress includes the annealing of hydrous RuO$_2 \cdot x$H$_2$O near the crystallization temperature,[17] combining with other conductive nanomaterials such as activated carbon, carbon nanotubes, and graphene,[18–24]

Interdisciplinary School of Green Energy, KIER-UNIST Advanced Center for Energy and Low Dimensional Carbon Materials Center, Ulsan National Institute of Science and Technology (UNIST), Ulsan 689-798, Korea. E-mail: bskim19@unist.ac.kr; Fax: +82-52-217-2019; Tel: +82-52-217-2923

† Electronic supplementary information (ESI) available: FT-IR spectra of PEO-*b*-PAA at each step and RuO$_2$ nanoparticles after thermal annealing, *in situ* XRD patterns and TEM images of RuO$_2$ nanoparticles at different temperatures and Nyquist plots of as-prepared RuO$_2$ and RuO$_2$ annealed at 400 °C as an electrode. See DOI: 10.1039/c2jm30738c

and designing new architectures like nanotubes[9,25] and nano-fibers of conductive networks.[17] Many of these approaches find their utilities in enhancing the specific capacitance; however, it is still challenging to retain the high capacitance of RuO_2 while achieving both good proton permeation and electronic conduction without an additional matrix.

Herein, we present the unique use of double hydrophilic block copolymer (DHBC) both as a soft template to prepare the hydrous RuO_2 nanoparticles with a controlled dimension and as a surface modifier to significantly increase the ionic conductivity of the resulting nanoparticles after thermal annealing. Specifically, the DHBC of poly(ethylene oxide)-*block*-poly(acrylic acid) (PEO-*b*-PAA) was employed to form a micelle upon addition of the ruthenium precursor, $RuCl_3 \cdot xH_2O$, which then transformed into hydrous RuO_2 nanoparticles of a controlled dimension using a reducing agent (Scheme 1). Furthermore, upon annealing of as-prepared RuO_2 nanoparticles at 400 °C, we find that the crystallinity of RuO_2 nanoparticles increases with a simultaneous transformation of the surrounding DHBC into ionic and electronic conducting buffer layers atop RuO_2 nanoparticles, which contribute to the significant enhancement of the overall specific capacitance of 962 F g^{-1} at a scan rate of 10 mV s^{-1} with excellent cycle life.

This DHBC-based method offers a unique and facile solution-based synthesis of nanoparticles under mild conditions and does not require any foreign materials to increase the capacitance as well as to improve the rate capability during the charging–discharging process. To the best of our knowledge, this is *the first example* of employing DHBCs in the synthesis of RuO_2 nanoparticles and their application in supercapacitors. Because the self-assembly of DHBC with a metal precursor relies solely on the electrostatic interactions, we argue that this method can be readily extended to other nanoparticles of controlled dimensions and structures. We envision that the DHBC will provide a facile and general tool in creating functional nanostructures for various applications.

2. Experimental section

Materials

Ruthenium(III) chloride hydrate ($RuCl_3 \cdot xH_2O$) and hydrazine (NH_2NH_2) were purchased from Aldrich and used without further purification. A double hydrophilic block copolymer of PEO(5000)-*b*-PAA(6700) was purchased from Polymer Source, Inc.

Synthesis of hydrous $RuO_2 \cdot xH_2O$ nanoparticles

The ruthenium oxide nanoparticles were prepared according to the following protocols. First, a double hydrophilic block copolymer of PEO(5000)-*b*-PAA(6700) (25.12 mg, 0.20 mmol of carboxylic acid groups) and $RuCl_3 \cdot xH_2O$ (17.8 mg, 0.10 mmol) in 5.0 mL of deionized water were prepared separately and mixed under vigorous stirring. To this solution mixture, 0.10 mL of 4.0 M NaOH (0.40 mmol, 2 equiv. to carboxylic acid groups) was added and the color in the solution changed from black to dark cyan. Subsequently, 0.10 mL of 10.0 M hydrazine (1.0 mmol) was added dropwise to the resulting suspensions under vigorous stirring. As soon as the hydrazine is added, the solution color turns into light cyan. After 30 min of vigorous stirring, the solution mixture was centrifuged to remove large aggregates of nanoparticles (1500 rpm, 15 min), and then the recovered supernatant was dialyzed against deionized water using a dialysis membrane (MWCO 12 000–14 000, SpectraPore) for 6 h to remove any byproduct and residuals. The prepared suspension of $RuO_2 \cdot xH_2O$ nanoparticles exhibited a fairly good colloidal stability for more than 6 months without any precipitation. For annealing, the RuO_2 powder was first obtained by using a freeze dryer and this powder was subjected to annealing at different temperatures for 2 h in a muffle furnace under air atmosphere.

Characterization

The morphology, size, and size distributions of the prepared nanoparticles were investigated using transmission electron microscopy (TEM, JEOL JEM-2100, accelerating voltage of 200 kV, Gatan CCD camera). X-ray diffraction (XRD) measurements were carried out with a high-power X-ray diffractometer (Rigaku Co., D/MAZX 2500V/PC) from 10° to 90°. X-ray photoelectron spectroscopy (XPS) measurements were performed on a Thermo Fisher, K-alpha. Thermogravimetric analysis (TGA) was conducted in air atmosphere at a heating rate of 10 °C min^{-1} using a thermogravimetric analyzer (Q200, TA Instruments). Fourier-transform infrared (FT-IR) spectra were obtained with a FT-IR spectrophotometer (Varian).

Electrochemical measurements

The working electrode was prepared by loading the prepared sample on the surface of quartz crystal microbalance (QCM) substrate coated with gold. Then, the weight of RuO_2 loaded on the surface of electrode was calculated from the frequency of
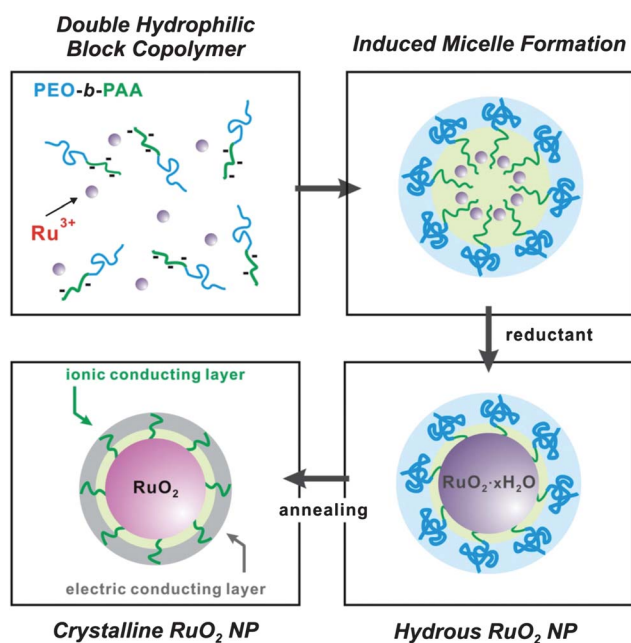
Scheme 1 Schematic illustration of synthesis of RuO_2 nanoparticles using a double hydrophilic block copolymer as a template and resulting nanostructures after annealing at high temperature.

This journal is © The Royal Society of Chemistry 2012

J. Mater. Chem., 2012, **22**, 11598–11604 | 11599

eQCM (SEIKO, EG&G, QCA922-00). The electrochemical properties of RuO_2 electrodes were characterized by means of cyclic voltammetry and a galvanostat (BioLogic, VSP) at ambient temperature. The CV measurements were carried out using a three-electrode cell, in which a platinum wire was used as a counter-electrode and the saturated calomel electrode (SCE) as a reference electrode, in the potential range between -0.1 and $+0.9$ V with scan rates from 10 to 200 mV s^{-1} in an aqueous 1.0 M H_2SO_4 solution. The charge–discharge galvanostatic tests were performed at current densities from 3 to 20 A g^{-1}.

3. Results and discussion

Synthesis and characterization of hydrous RuO_2 nanoparticles

The synthesis of RuO_2 nanoparticles by DHBCs is illustrated in Scheme 1. Traditionally, DHBCs have been employed in the growth control of inorganic mineralization with unusual structural specialty and complexity in aqueous solutions such as $CaCO_3$, $BaSO_4$, and $Ca_3(PO_4)_2$;[26,27] however, there are only a few examples of employing the DHBCs in the synthesis of nanoparticles.[28–30] In our approach, we use PEO-b-PAA that consists of a binding ionizable PAA block and a solvating neutral PEO block, as stabilizers for the controlled synthesis of hydrous RuO_2 nanoparticles. Upon introduction of Ru^{3+} ions that interact with the ionizable PAA block in solution via electrostatic interactions, the PAA blocks are promoted to the formation of micellar aggregates in solution. The formation of micellar colloids with a similar core–shell structure was proposed with other metal ions complexing with DHBCs in previous reports.[31,32] Once the micelle formation is induced, the PEO-b-PAA micelle acts as a nanoreactor to control the nanoparticle growth within the micellar core with the addition of a reducing agent, N_2H_4. The prepared homogeneous suspension of RuO_2 nanoparticles remains stable for several months without noticeable aggregates due to the PEO block that are sterically stabilizing the nanoparticles in aqueous solution (Fig. 1). A control experiment of using only a PAA polymer of a similar molecular weight does not yield the stable suspension of hydrous RuO_2 nanoparticles, highlighting the important role of the PEO block in stabilizing the nanoparticles. In addition, the selective interaction between the ionizable block of PAA and the Ru metal precursor was confirmed by the FT-IR spectra. The peak at 1570 cm^{-1} attributed to the stretching vibration of the carboxylate groups (COO$^-$) in PAA is considerably diminished after the addition of Ru^{3+}, while the peak at 1104 cm^{-1} from the ether group (C–O–C) in the PEO block does not change at all, suggesting the preferential interaction between PAA and the metal precursor is dominant as presented in Scheme 1 (Fig. S1†).

The morphology and structure of the RuO_2 nanoparticles formed are investigated with transmission electron microscopy (TEM) (Fig. 1), X-ray photoelectron spectroscopy (XPS) and X-ray diffraction (XRD) (Fig. 2). The TEM image of the as-prepared RuO_2 nanoparticles shows a spherical shape of the RuO_2 nanoparticles with an average diameter of 1.9 ± 0.63 nm. The average diameter of RuO_2 nanoparticles is also tunable with varying ratios of metal precursor to DHBC in the range of $ca.$ 1–3 nm (data not shown). Although the high-resolution TEM reveals the crystalline lattice fringe of 0.224 nm from some
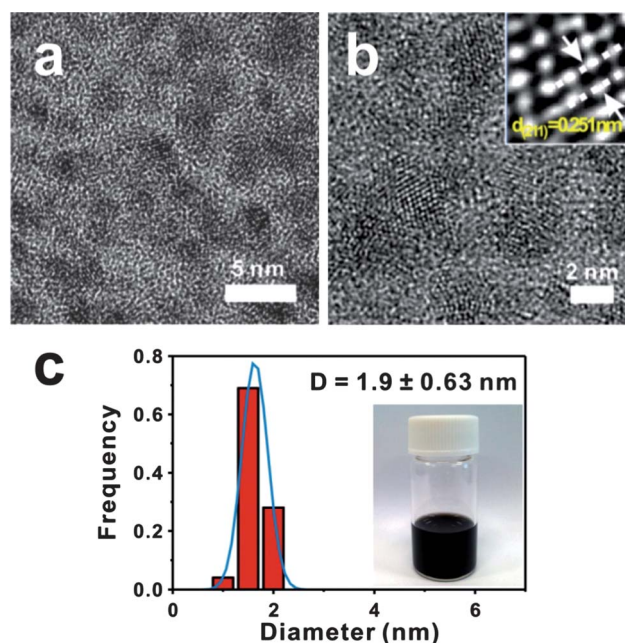
Fig. 1 (a and b) TEM images of as-prepared hydrous $RuO_2 \cdot xH_2O$ nanoparticles. The inset in Fig. 1b shows the crystalline lattice fringe of $RuO_2 \cdot xH_2O$ nanoparticles. (c) Corresponding size distribution histogram with an image of as-prepared hydrous $RuO_2 \cdot xH_2O$ nanoparticle suspension.

nanoparticles, which corresponds to the primary reflection of the (211) peak of RuO_2 nanoparticles, the XRD does not indicate the crystallinity of the RuO_2 nanoparticles prepared, suggesting the formation of amorphous $RuO_2 \cdot xH_2O$ nanoparticles. This is consistent with other studies of synthesizing RuO_2 nanoparticles under mild reaction temperature.[33,34]

XPS further reveals the oxidation status of as-prepared $RuO_2 \cdot xH_2O$ nanoparticles after the deconvolution of the peaks (Fig. 2a). Though the Ru3$d_{5/2}$ and 3$d_{3/2}$ signals are overlapping with the C1s peak centered at 284.0 eV, the signals at 280.9 and 285.6 eV can be assigned to Ru(IV) of RuO_2. The other two signals at 283.1 and 287.8 eV are characteristic of Ru(III) corresponding to hydrous Ru(III)–OH.[25] Moreover, the deconvoluted high-resolution O1s spectra of as-prepared $RuO_2 \cdot xH_2O$ nanoparticles exhibited three distinct components, including lattice oxygen O^{2-} in RuO_2 (530.2 eV), hydroxyl (532.0 eV), and surface bound H_2O (533.9 eV), which are all in good agreement with previous reports. Collectively, the TEM and XPS data support the successful formation of hydrous $RuO_2 \cdot xH_2O$ nanoparticles with the DHBC template.

As introduced, careful control over the degree of crystallinity and hydration is essential for reaching high capacitance with enhanced cycle life that is related to the electrical and electrochemical properties of RuO_2-based materials. Thus, as-prepared hydrous $RuO_2 \cdot xH_2O$ nanoparticles were subjected to thermal annealing under different temperatures (200 to 600 °C) for 2 h to tune the level of crystallinity and the hydration of the RuO_2 nanoparticles and XRD followed to elucidate these changes in RuO_2 nanoparticles (Fig. 2b).

As shown in Fig. 2, the crystallinity of RuO_2 nanoparticles increases considerably upon annealing at high temperature. For
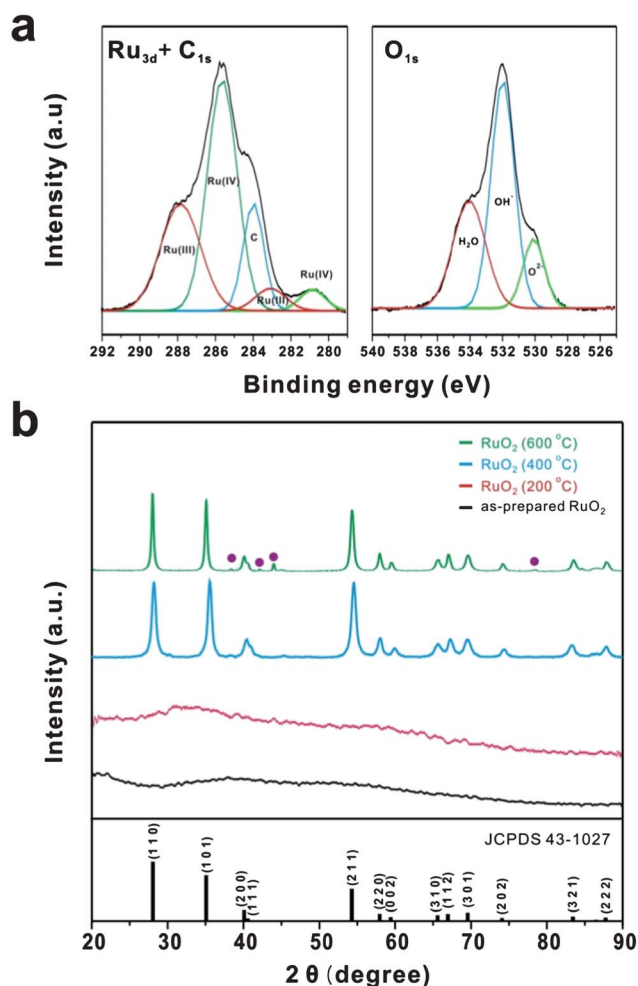
Fig. 2 (a) Deconvoluted high-resolution XPS spectra of as-prepared hydrous $RuO_2 \cdot xH_2O$ nanoparticles. (b) XRD spectra of various RuO_2 nanoparticles before and after annealing at different temperatures. Note the circles in (b) represent the peak matching to metallic ruthenium.

example, the peaks related to the rutile phase of RuO_2 such as (101), (110), and (211) begin to evolve after heat treatment at 300 °C and become apparent after annealing beyond 400 °C (Fig. S2†). While annealing of as-prepared hydrous $RuO_2 \cdot xH_2O$ nanoparticles crystallized the inorganic network, the organic DHBC micelles surrounding the RuO_2 nanoparticles also began to decompose, resulting in an amorphous carbon layer on top of RuO_2 nanoparticles, which is not clearly discernible by XRD. Moreover, it should be noted that there are still some polymeric layers remaining even after annealing at 400 °C, as evidenced by the presence of residual polymeric layers using FT-IR, including symmetric stretching of carboxylate peaks from PAA at 1435 cm^{-1} and strong rocking of the PAA backbone at 863 cm^{-1}, which reflect the surface-bound strong coordinating carboxylate groups in PAA (Fig. S3†). In contrast, we could not observe any residual peaks relevant to the PEO block after thermal annealing above 400 °C, suggesting that the selective degradation of the PEO block took place below 400 °C. It turns out that this residual polymeric layer of DHBC, which mainly consists of PAA block and amorphous carbon layer, serves a critical role in increasing the ionic and electronic conduction pathways during electrochemical cycles.

Taken together, we postulate that as-prepared hydrous RuO_2 nanoparticles undergo phase transition from amorphous to crystalline state upon thermal annealing with the formation of a residual polymeric layer on top of nanoparticles. TEM measurements also indicate that the size of nanoparticles increases gradually with the progress of annealing (Fig. S4†).

The thermal stability as well as the relative content of the polymer in the as-prepared $RuO_2 \cdot xH_2O$ nanoparticles was estimated based on the thermogravimetric analysis (TGA) measurement (Fig. 3). As shown in the TGA curve of as-prepared hydrous $RuO_2 \cdot xH_2O$ nanoparticles, an initial mass loss of water at around 62.8 °C was observed. Followed by the initial mass loss, the second mass loss began at around 250 °C, which is associated with the degradation of DHBCs. Subsequently, characteristic peaks in the range of 300–400 °C were observed according to the differential TGA curve, which are attributed to the removal of crystalline water in hydrous RuO_2,[24,35] suggesting that the initially formed amorphous hydrous RuO_2 was transformed into a crystalline phase near 400 °C. As stated in the description of XRD, the existence of residual polymers at 400 °C is clearly evidenced by the presence of the peak near 607 °C, indicating the complete degradation of DHBCs at this temperature. The subsequent weight loss corresponds to the conversion of residual DHBCs into an amorphous carbonaceous layer on top of nanoparticles, which leads to approximately 38% of RuO_2
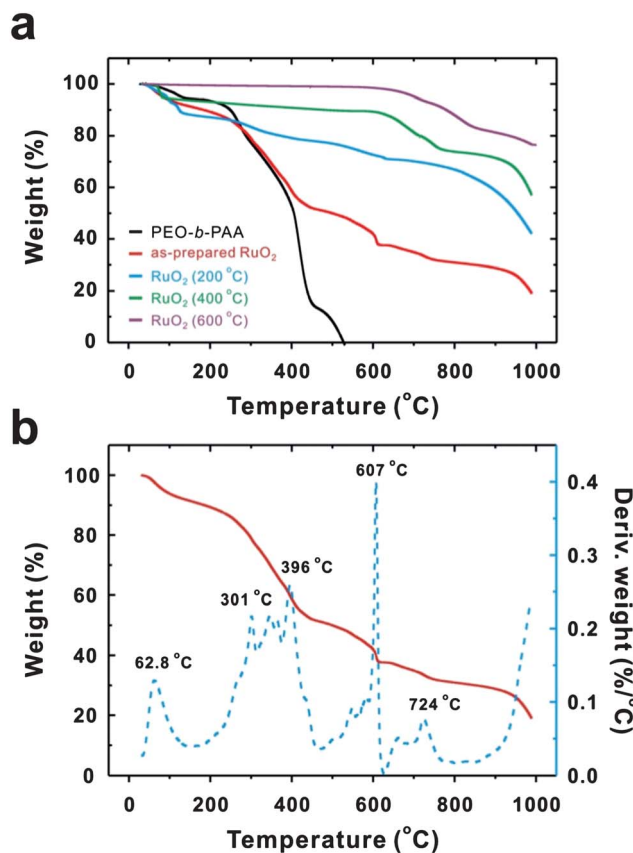
Fig. 3 (a) Thermogravimetric analysis (TGA) and (b) differential thermal analysis (DTA) curves of as-prepared hydrous $RuO_2 \cdot xH_2O$ nanoparticles. The sample was subjected to heating at a rate of 10 °C min^{-1} under air atmosphere.

This journal is © The Royal Society of Chemistry 2012

J. Mater. Chem., 2012, 22, 11598–11604 | 11601

being present within the resulting nanocomposite. RuO_2 nanoparticles annealed at higher temperatures generally yield more amount of nanoparticles with respect to the polymer content from 19% (as-prepared) to 76% (annealed at 600 °C), as the polymer decomposed during the annealing process. In concert with the FT-IR data, TGA also indicated that the specific interaction between the polymer and the metal precursor increased the degradation temperature of pure PEO-b-PAA from 525 to 611 °C. This also demonstrates the strong interaction between the metal ions and DHBCs.

Electrochemical behavior of RuO_2 electrode in supercapacitor

The capacitive performance of the prepared RuO_2 nanoparticles was evaluated by using cyclic voltammetry (CV) (Fig. 4). Fig. 4 shows the CV results of all RuO_2 nanoparticles prepared before and after the annealing at different temperatures, which were measured in 1.0 M H_2SO_4 at potential intervals from −0.1 to 0.9 V using the saturated calomel electrode (SCE) as a reference electrode. All samples exhibit broad redox peaks in the potential range investigated, which displays a typical pseudocapacitive behavior of RuO_2 nanoparticles. The specific capacitance (C_{sp}) was calculated by the following equation:[23]

$$C_{sp} = \frac{1}{mv(V_f - V_i)} \int_{V_i}^{V_f} I(V)\,dV, \quad (1)$$

where m is the mass of the active electrode materials measured by the quartz crystal microbalance (QCM), v is the scan rate, V is the integration potential limit, and $I(V)$ is the voltammetric current. As shown in Fig. 4, the specific capacitances of as-prepared RuO_2, annealed at 200, 400, and 600 °C obtained at 10 mV s^{-1} are 106, 358, 962, and 25 F g^{-1}, respectively. As-prepared hydrous $RuO_2 \cdot xH_2O$ nanoparticles within a polymeric shell of DHBC did not show a noticeable capacitive activity possibly due to the existence of DHBCs on top of the nanoparticles which prevent the effective current pathway. On the other hand, the samples after annealing generally show the significantly enhanced capacitance values and, to our surprise, the sample annealed at 400 °C exhibits an outstanding specific capacitance of 962 F g^{-1} at a scan rate of 10 mV s^{-1} and even shows the specific capacitance of 430 F g^{-1} at a fast scan rate of 200 mV s^{-1}. Besides, a linear response of the capacitive current with respect to the potential scan rate reveals the high reversibility of the system. Furthermore, it is important to note that the capacitance loss of the sample at a high scan rate is still moderate
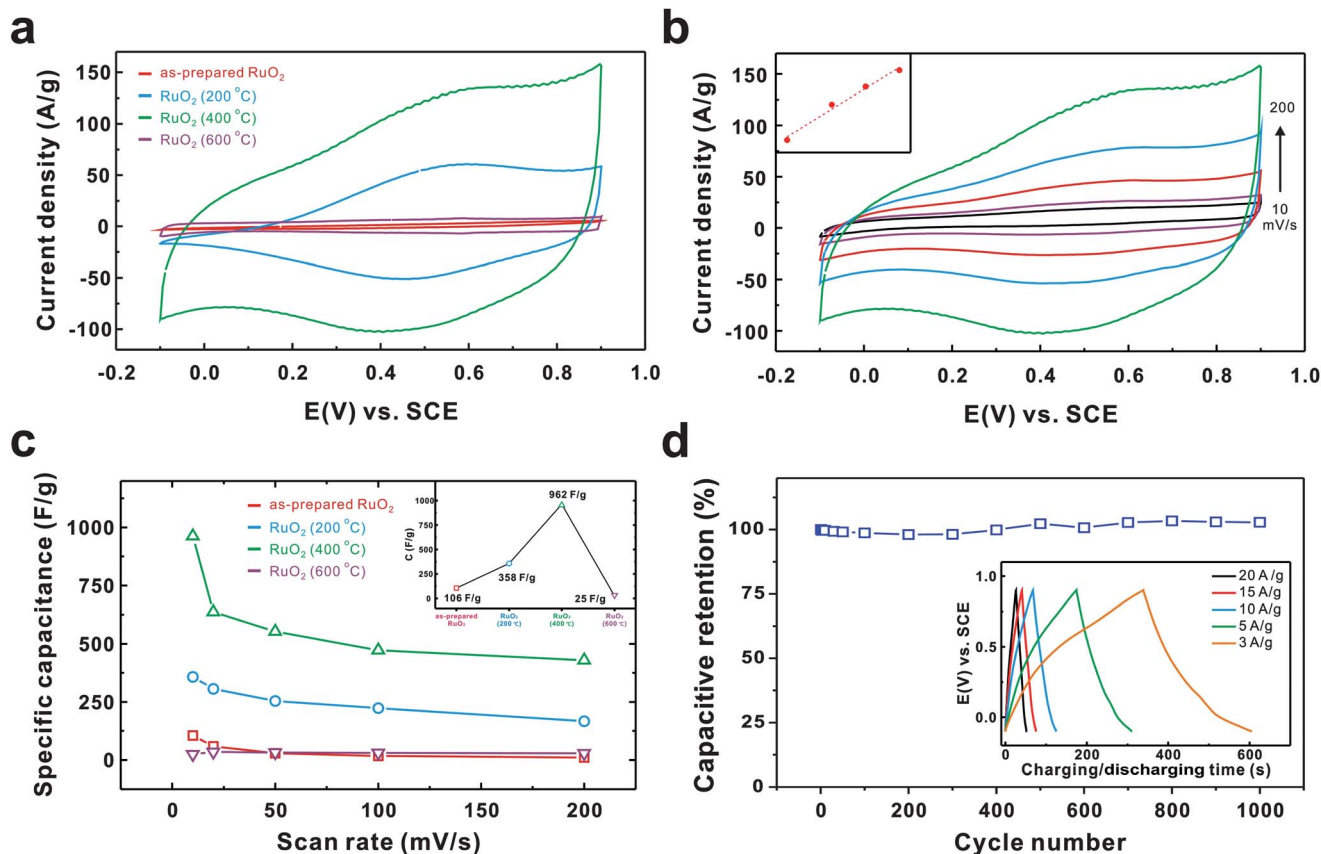
Fig. 4 Comparison of electrochemical properties of all RuO_2 nanoparticle samples. (a) Cyclic voltammograms (CVs) of RuO_2 nanoparticle electrodes at a scan rate of 200 mV s^{-1}; (b) scan rate dependent current density plot of RuO_2 nanoparticles after annealing at 400 °C with a scan rate of 10, 20, 50, 100, and 200 mV s^{-1}, the inset shows the peak current density *versus* scan rate plot in an equi-span log–log scale with a calculated slope of 1.0; (c) dependence of the capacitance loss on the scan rate of all RuO_2 nanoparticle samples with an inset of capacitance values at a scan rate of 10 mV s^{-1}; and (d) galvanostat cycling of RuO_2 after annealing at 400 °C with a current density of 20 A g^{-1}, the inset shows the charge–discharge curves with various current densities. All electrochemical properties were collected in a three-electrode system with a SCE reference in 1.0 M H_2SO_4 electrolyte.

compared to other samples. This considerable difference in the specific capacitance is mainly attributed to the degree of crystallinity as well as the hydration, and most importantly, the role of residual DHBC in enhancing the ionic and electronic conductivities of the materials at the interface between the RuO_2 nanoparticles and H_2SO_4 electrolyte. The sample annealed at a higher temperature of 600 °C, however, displays a poor capacitance of 25 F g^{-1} even at a higher crystallinity of RuO_2 nanoparticles. This is primarily attributed to the dense crystalline structure of RuO_2 as well as the disappearance of the residual ionic conducting layer on top of RuO_2 nanoparticles, which hamper the effective transport of protons upon complete removal of DHBCs. This is in accord with the high-resolution TEM image showing the highly crystalline carbon layer on top of RuO_2 nanoparticles (Fig. S5†).

Finally, we evaluated the cycling stability of the RuO_2 nanoparticles annealed at 400 °C using a galvanostat charge–discharge test under the identical three-electrode system. As shown in Fig. 4d, the non-linear charge–discharge curve featured the characteristic pseudocapacitive behavior of the sample. The specific capacitance of the supercapacitor was calculated to be 800 F g^{-1} at a current density of 3 A g^{-1}, which is similar to that obtained from the CV measurement. This value is comparable to the recent study of Sassoye and co-workers reporting a RuO_2-based mesoporous thin film prepared by an amphiphilic block copolymer, PS-*b*-PEO, having a capacitance of 1000 ± 100 F g^{-1} and the other study of Huang and co-workers reporting a capacitance of 653 F g^{-1} from hydrous RuO_2 loaded into a PEDOT:PSS matrix.[15,36] Most notably, the excellent cycle life of the electrode is demonstrated with the 100% retention of capacitance even after 1000 cycles at a high current density of 20 A g^{-1}. It has been often observed that the RuO_2 nanoparticles often undergo irreversible aggregation after cycles of charging–discharging, which may significantly degrade their electrochemical redox processes at the interface with the electrolytes. However, in this case, the residual polymeric layer on top of RuO_2 nanoparticles not only prevents the re-aggregation of the active nanoparticles, but also provides an intimate ionic and electronic conducting pathway with electrolytes, leading to the rapid and efficient redox reactions on the surface of RuO_2 nanoparticles (Fig. 5). Further electrochemical impedance measurements also support the markedly increased electrochemical property of RuO_2 nanoparticles annealed at 400 °C

compared to that of as-prepared hydrous $RuO_2 \cdot xH_2O$ nanoparticles (Fig. S6†). Although more stringent tests are still required, we have further optimized the current annealing temperature to different ranges near 400 °C and found that annealing of hydrous $RuO_2 \cdot xH_2O$ nanoparticles at 350 °C yielded a capacitance of even to 1070 F g^{-1} at a scan rate of 10 mV s^{-1}, which is about 11% capacitance increase compared to annealing at 400 °C (Fig. S7†).

4.   Conclusion

In summary, we have developed a facile synthesis of ruthenium oxide (RuO_2) nanoparticles using a double hydrophilic block copolymer, PEO-*b*-PAA, as a soft template and demonstrated its promising potential for supercapacitors. The stable suspension of hydrous $RuO_2 \cdot xH_2O$ nanoparticles of a controlled dimension was prepared under a mild aqueous condition. Furthermore, we found that upon annealing as-prepared hydrous $RuO_2 \cdot xH_2O$ nanoparticles at 400 °C, the crystallinity of RuO_2 nanoparticles increased with a simultaneous transformation of the surrounding DHBC into an ionic conducting buffer layer atop RuO_2 nanoparticles, which contributed to the significant enhancement of the overall specific capacitance of 962 F g^{-1} at a scan rate of 10 mV s^{-1} with an excellent cycle life over 1000 times. Because the self-assembly of DHBCs with a metal precursor relies solely on the electrostatic interactions, we argue that this method can be readily extended to other nanoparticles of controlled dimensions and structures. We envision that the DHBC will provide a facile and general means of creating other functional nanostructures for various applications.

Acknowledgements

References

1 B. E. Conway, *Electrochemical Supercapacitors: Scientific Fundamentals and Technological Applications*, Kluwer Academic/Plenum, New York, 1999.
2 A. S. Arico, P. Bruce, B. Scrosati, J. M. Tarascon and W. Van Schalkwijk, *Nat. Mater.*, 2005, **4**, 366.
3 P. J. Hall, M. Mirzaeian, S. I. Fletcher, F. B. Sillars, A. J. R. Rennie, G. O. Shitta-Bey, G. Wilson, A. Cruden and R. Carter, *Energy Environ. Sci.*, 2010, **3**, 1238.
4 C. Liu, F. Li, L. P. Ma and H. M. Cheng, *Adv. Mater.*, 2010, **22**, E28.
5 P. Simon and Y. Gogotsi, *Nat. Mater.*, 2008, **7**, 845.
6 M. D. Stoller and R. S. Ruoff, *Energy Environ. Sci.*, 2010, **3**, 1294.
7 B. Conway, V. Birss and J. Wojtowicz, *J. Power Sources*, 1997, **66**, 1.
8 C. C. Hu, K. H. Chang, M. C. Lin and Y. T. Wu, *Nano Lett.*, 2006, **6**, 2690.
9 R. Liu, J. Duay, T. Lane and S. B. Lee, *Phys. Chem. Chem. Phys.*, 2010, **12**, 4309.
10 X. Liu and P. G. Pickup, *Energy Environ. Sci.*, 2008, **1**, 494.
11 D. Susanti, D. S. Tsai, Y. S. Huang, A. Korotcov and W. H. Chung, *J. Phys. Chem. C*, 2007, **111**, 9530.
12 J. S. Ye, H. F. Cui, X. Liu, T. M. Lim, W. D. Zhang and F. S. Sheu, *Small*, 2005, **1**, 560.
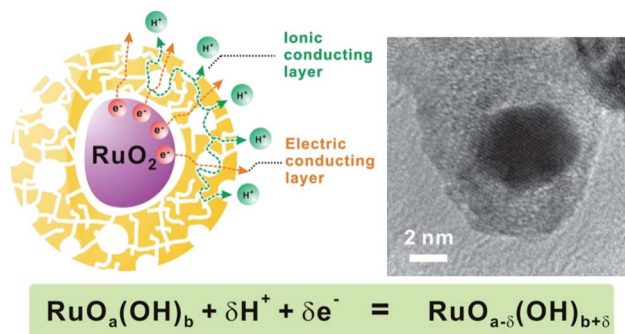
Fig. 5 Schematic representation of the origin of enhanced capacitive performance of RuO_2 nanoparticles annealed at 400 °C with the corresponding TEM image.

This journal is © The Royal Society of Chemistry 2012

J. Mater. Chem., 2012, **22**, 11598–11604 | 11603

13 K. H. Chang and C. C. Hu, *Electrochem. Solid-State Lett.*, 2004, **7**, A466.

14 K. H. Chang and C. C. Hu, *J. Electrochem. Soc.*, 2004, **151**, A958.

15 C. Sassoye, C. Laberty, H. Le Khanh, S. Cassaignon, C. Boissière, M. Antonietti and C. Sanchez, *Adv. Funct. Mater.*, 2009, **19**, 1922.

16 J. Zheng, P. Cygan and T. Jow, *J. Electrochem. Soc.*, 1995, **142**, 2699.

17 T. S. Hyun, H. L. Tuller, D. Y. Youn, H. G. Kim and I. D. Kim, *J. Mater. Chem.*, 2010, **20**, 9172.

18 Y. Su, F. Wu, L. Bao and Z. Yang, *New Carbon Mater.*, 2007, **22**, 53.

19 J. Zhang, D. Jiang, B. Chen, J. Zhu, L. Jiang and H. Fang, *J. Electrochem. Soc.*, 2001, **148**, A1362.

20 G. Arabale, D. Wagh, M. Kulkarni, I. Mulla, S. Vernekar, K. Vijayamohanan and A. Rao, *Chem. Phys. Lett.*, 2003, **376**, 207.

21 W. C. Fang, O. Chyan, C. L. Sun, C. T. Wu, C. P. Chen, K. H. Chen, L. C. Chen and J. H. Huang, *Electrochem. Commun.*, 2007, **9**, 239.

22 Y. T. Kim, K. Tadai and T. Mitani, *J. Mater. Chem.*, 2005, **15**, 4914.

23 Z. S. Wu, D. W. Wang, W. Ren, J. Zhao, G. Zhou, F. Li and H. M. Cheng, *Adv. Funct. Mater.*, 2010, **20**, 3595.

24 J. Zhang, J. Jiang, H. Li and X. Zhao, *Energy Environ. Sci.*, 2011, **4**, 4009.

25 J. Zhang, J. Ma, L. L. Zhang, P. Guo, J. Jiang and X. Zhao, *J. Phys. Chem. C*, 2011, **114**, 13608.

26 H. Cölfen, *Macromol. Rapid Commun.*, 2001, **22**, 219.

27 K. Nakashima and P. Bahadur, *Adv. Colloid Interface Sci.*, 2006, **123**, 75.

28 A. Kim, B. Sharma, B. S. Kim and K. H. Park, *J. Nanosci. Nanotechnol.*, 2011, **11**, 6162.

29 L. Qi, H. Cölfen and M. Antonietti, *Nano Lett.*, 2001, **1**, 61.

30 A. Taubert, D. Palms, Ö. Weiss, M. T. Piccini and D. N. Batchelder, *Chem. Mater.*, 2002, **14**, 2594.

31 F. Bouyer, N. Sanson, M. Destarac and C. Gérardin, *New J. Chem.*, 2006, **30**, 399.

32 L. Bronstein, S. Sidorov, A. Gourkova, P. Valetsky, J. Hartmann, M. Breulmann, H. Colfen and M. Antonietti, *Inorg. Chim. Acta*, 1998, **280**, 348.

33 T. Gujar, V. Shinde, C. Lokhande, W. Y. Kim, K. D. Jung and O. S. Joo, *Electrochem. Commun.*, 2007, **9**, 504.

34 J. Walker, R. Bruce King and R. Tannenbaum, *J. Solid State Chem.*, 2007, **180**, 2290.

35 J. P. Zheng, *J. Electrochem. Soc.*, 2009, **156**, A500.

36 L. M. Huang, H. Z. Lin, T. C. Wen and A. Gopalan, *Electrochim. Acta*, 2006, **52**, 1058.